Recovering Missing Slices of the Discrete Fourier Transform using Ghosts

Shekhar S. Chandra, *Member, IEEE*, Imants Svalbe, Jeanpierre Guédon, Andrew Kingston and Nicolas Normand

***Abstract*—The Discrete Fourier Transform (DFT) underpins the solution to many inverse problems commonly possessing missing or un-measured frequency information. This incomplete coverage of Fourier space always produces systematic artefacts called Ghosts. In this paper, a fast and exact method for deconvolving cyclic artefacts caused by missing slices of the DFT using redundant image regions is presented. The slices discussed here originate from the exact partitioning of DFT space, under the projective Discrete Radon Transform, called the Discrete Fourier Slice Theorem. The method has a computational complexity of $O(n \log_2 n)$ (for an $n = N \times N$ image) and is constructed from a new cyclic theory of Ghosts. This theory is also shown to unify several aspects of work done on Ghosts over the past three decades. The paper concludes with an application to fast, exact, non-iterative image reconstruction from a highly asymmetric set of rational angle projections that give rise to sets of sparse slices within the DFT.**

***Index Terms*—Discrete Radon Transform, Mojette Transform, Discrete Tomography, Image Reconstruction, Discrete Fourier Slice Theorem, Ghosts, Number Theoretic Transform, Limited Angle, Cyclic Ghost Theory**

I. Introduction

The Discrete Fourier Transform (DFT) is an important tool for inverse problems, where the discrete Fourier representation of an object is used as a mechanism to recover that object. The Discrete Fourier Slice Theorem (FST) property of the DFT, independently developed by Grigoryan and others [1–4], is especially important for discrete tomographic inverse problems, where a discrete object can be recovered exactly from its discrete projected "views" or projections [5].

The Discrete FST provides an exact partitioning of two dimensional (2D) DFT space into a finite number of one dimensional (1D) discrete "slices" of equal length. These slices have discrete slopes m and s with $m, s \in \mathbb{N}_0$, wrapping around DFT space in both rows and columns, while tiling the space perfectly without interpolation [6]. The partitioning is valid for $N \times N$ spaces, where $N = p^n$, p is prime, $n \geqslant 1$ and $p, n \in \mathbb{N}_0$. This includes prime sizes [7], power of two sizes [8–10] and has also been generalised to composite N [11, 7]. Rectangular spaces can be handled by zero-padding them to the nearest square size. A total of $N + N/p$ slices is required to tile all of 2D DFT space exactly [7]. Fig. 1 gives an example of this slice partitioning when N is prime.

 S. S. Chandra (Shekhar.Chandra@csiro.au) is with the Australian e-Health Research Centre, CSIRO, Australia. I. Svalbe (Imants.Svalbe@monash.edu) is with Monash University, Australia. A. Kingston is with Australian National University, Australia. J. Guédon and N. Normand are with LUNAM Université, Université de Nantes, IRCCyN UMR CNRS 6597, Nantes, France.

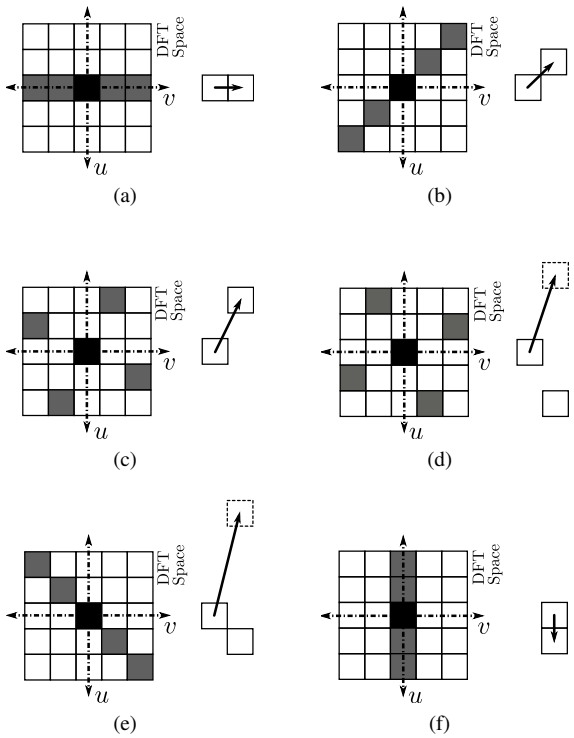

Figure 1. The slices of the DFT having a square size of length $N = 5$. Grey pixels in (a)-(e) and (f) each represent a slice of different discrete slopes m and s respectively (indicated by their accompanying vectors $[-m, 1]$ and $[1, -ps]$) with the DC coefficient centred (black). Note that each slice wraps around DFT space (i.e. computed modulo N) and the six slices tile all of 2D DFT space at least once without interpolation.

The inverse DFT (iDFT) of the slices corresponds directly to the projections of the Discrete Radon Transform (DRT) [6]. These projections are computed as sums along the lines formed by the vectors $[1, m]$ and $[ps, 1]$, i.e. m pixels across and one pixel down or one pixel across and ps pixels down. Fig. 2 gives the equivalent projections for the slices of the DFT shown in Fig. 1. The DRT projections are normally ordered by slope and translate t, and is often referred to as DRT space. Fig. 3(a) shows the DRT space of an image of Lena.

By computing $N + N/p$ DRT projections with the set of slopes $\boldsymbol{m}$ and $\boldsymbol{s}$ as

$$\boldsymbol{m} = \{m : m < N,\ m \in \mathbb{N}_0\}, \quad (1)$$

$$\boldsymbol{s} = \{s : s < N/p,\ s \in \mathbb{N}_0\}, \quad (2)$$

and the set of translates or intercepts $\boldsymbol{t}$ as

$$\boldsymbol{t} = \{t : t < N,\ t \in \mathbb{N}_0\}, \quad (3)$$

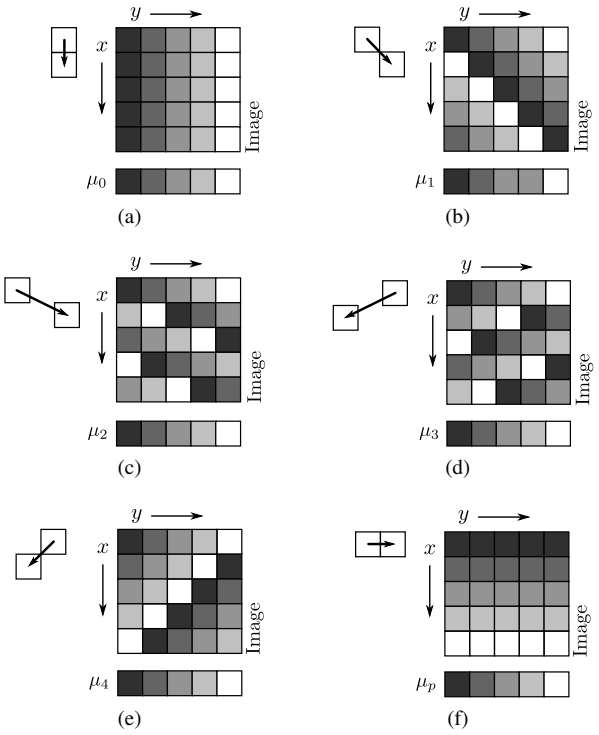

Figure 2. The projections of the DRT that are equivalent to the slices shown in Fig. 1. (a)-(e) and (f) represent projections at different discrete slopes m and s (indicated by their accompanying vectors $[1, m]$ and $[ps, 1]$). Note that each projection wraps around image space (i.e. computed modulo N), the coordinate system of the projection vectors are perpendicular to the DFT space slice vectors and that each projection tiles all of image space at least once without interpolation.

where $x, y \in \mathbb{N}_0$, the 1D DFT of the projections can be placed into 2D DFT space directly (without interpolation) and the inverse 2D DFT utilised to recover the image. The slices are placed along the vectors $[-m, 1]$ and $[1, -ps]$ in 2D DFT space (see Fig. 1). For a prime-sized image, the result is normalised by subtracting the total image sum from each pixel (or equivalently correcting the DC coefficient in DFT space) and dividing by N. The reconstruction of the image is exact when there is no noise present in the projections.

It is common that not all projections are available to tile Fourier space in discrete tomographic inverse problems. This effectively means there are missing slices or projections, which introduce artefacts in the reconstruction known as discrete Ghosts [12]. Ghost artefacts have zero-sums in the projected directions of the missing data, so that their corresponding Fourier coefficients are also zero [12]. They may be superimposed on an image while still being invisible in the directions of the missing projections. Fig. 4 gives an example of what a Ghost can look like as an image.

Missing projections in the DRT produce cyclic artefacts on the reconstructed image [13, 14] and occur naturally when the DRT is applied to discrete tomography [13], image/erasure coding [15] and image processing [16]. Fig. 3(b) gives an example of missing projections and Ghosts in the DRT.

This paper presents a fast method for exactly removing Ghost artefacts formed from missing slices of the prime-sized DFT. The method utilises redundant or known image regions within the reconstruction to deconvolve these Ghosts artefacts. The method is constructed from a theory of cyclic Ghosts within the prime-sized Discrete FST that is also developed in this work. This theory for the Discrete FST is constructed using cyclic convolutions and results in algorithms of low computational complexity ($O(n \log_2 n)$ for an $n = N \times N$ image). A schematic summary of the process in given in Fig. 3(c). Finally, the Ghost deconvolution method is applied to exactly reconstruct images from a highly asymmetric set of rational angle projections that give rise to sets of sparse slices within the DFT.

The paper is structured as follows. Previous work on Ghosts and reconstructing from sparse signals is reviewed in the next section. This is followed by a theory of cyclic Ghosts for the Discrete FST in Sec. III. The convolution and deconvolution techniques for missing slices of the DFT is presented in Sec. IV. Finally, the results for applying these techniques in reconstructing an image exactly from a highly asymmetric set of rational angle projections is presented in Sec. V.

II. Previous Work

Bracewell and Roberts [17] introduced the concept of the "invisible distribution", later referred to as Ghosts by Katz [12] and Cornwell [18], in the context of the Fourier Transform (FT). These distributions are a consequence of non-unique solutions arising from an incomplete Fourier space or "u, v coverage" due to a finite number of measurements. Explicitly, a classical Ghost or invisible distribution exists where a continuous theory, i.e. one that utilises an integral transform, is the mechanism for an inverse problem. For example, the theory for Computed Tomography (CT) is commonly based on the FT, and is therefore ill-posed as a result and always has classical Ghosts [19]. Katz [12] rediscovered the concept of a Ghost and showed that Ghosts must have zero-sums in the directions of the missing projections.

Logan [20] presented the uncertainty principle for projections in the FT and determined that Ghosts are mostly present in the high frequencies. He proved why low-pass filtering of the projections, using filters such as the Ram-Lak [21] or Shepp-Logan [22] filters, is required when reconstructing from projections in the FT. These and other related filters are still being used today in modern CT [23]. Louis [24] reformulated this result in a simpler form using the Hankel Transform.

Katz [12] presented the uncertainty principle for discrete rational angle projections for square image sizes, where a projection is computed as sums along the lines formed by using the vector $[b, a]$ with $a, b \in \mathbb{Z}$. These acyclic projections constitute what is now known as the Mojette Transform (MT) [25]. Fig. 5 shows a simple example of a MT for a 4×4 image using three projections.

Katz [12] determined that an $N \times N$ image can be reconstructed exactly from a set of μ rational angle projections $[b_j, a_j]$ if and only if

$$N \leqslant \max\left(\sum_{j=0}^{\mu-1} |a_j|, \sum_{j=0}^{\mu-1} |b_j|\right). \tag{4}$$

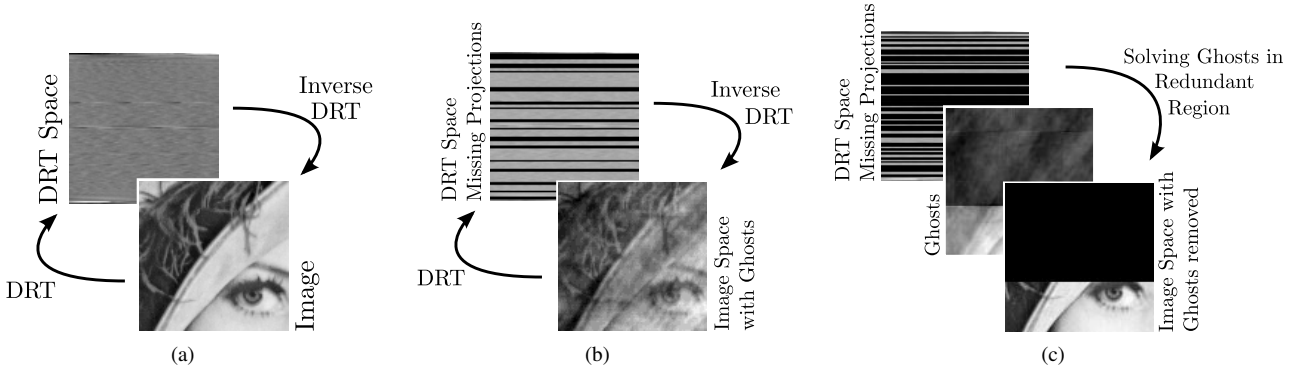

Figure 3. An illustration of the Discrete Radon Transform (DRT) and its cyclic Ghosts for an image of Lena. (a) shows the DRT space of the image of Lena and its one-to-one nature. (b) shows missing projections (black rows in DRT space) and their effect on the reconstructed image. (c) shows the result of deconvolving the Ghosts or "De-Ghosting" an image with Ghost artefacts in order to restore the image when a redundant image area is present.

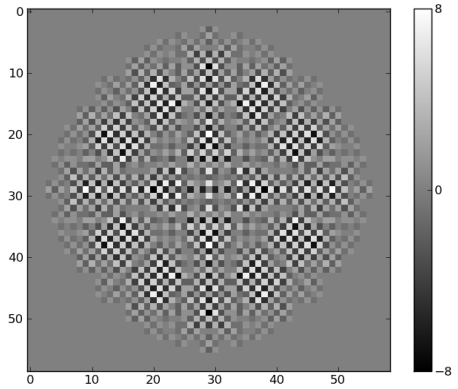

Figure 4. An example of a Ghost represented as an image. This Ghost is invisible at 24 rational angle projections and may be superimposed on an image without changing the projections of the image for these 24 angles.

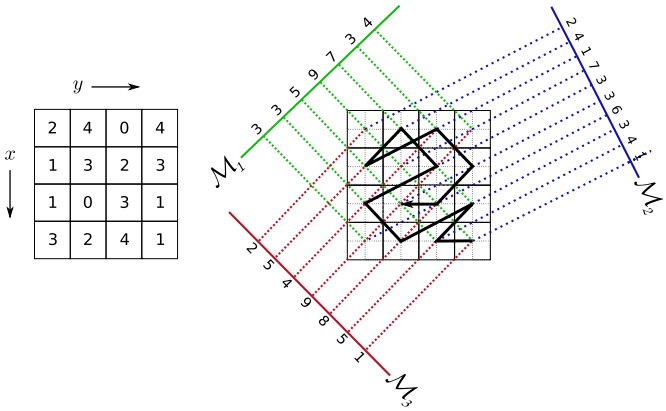

Figure 5. An example of a Mojette Transform for a discrete image of size 4×4 using the three projections $[1, 1]$, $[1, -1]$ and $[1, -2]$. The bold lines within the right-hand grid shows a possible reconstruction path using a corner-based reconstruction method [26].

This is now known as the Katz criterion. It is a statement that the information contained in the projection set needs to be one-to-one with the image data. When the criterion is not met, discrete Ghosts superimpose on the image because of the ambiguity in the projections [12]. These Ghosts look similar to the image in Fig. 4.

Normand *et al.* [27] extended the Katz criteria to arbitrary convex regions using mathematical morphology. They proved that a set of rational angle projections can only be reconstructed unambiguously if and only if the largest possible Ghost is larger than the convex region being reconstructed, so that there is no ghost present in the region due to the projection set. This less stringent criteria for the MT allows one to reconstruct images from a highly asymmetric set of projections [28]. These projections have a limited coverage in terms of the half-plane, i.e. the interval $[0, \pi)$, but are sufficient for an exact reconstruction in terms of the Katz criterion (4). A number of schemes have been proposed for these types of MT projections, including a Conjugate Gradient method [29] and a Geometric Graph approach [26], but the former is not suitably convergent and the latter is very sensitive to noise. Sec. V will present a fast alternative method based on the slices of the DFT and their Ghosts.

Highly asymmetric projection sets also occur in conventional limited angle tomography. Boyd and Little [30] presented a solution to limited angle tomography by reducing Ghosts through the fusion of multi-modal data to improve Fourier coverage. Techniques that minimise the L_1-norm are a common approach to reduce Ghost artefacts in reconstructions [31–34]. Vetterli *et al.* [35] showed that $\mathcal{N}$ spikes can be recovered exactly from $2\mathcal{N}+1$ consecutive Fourier samples by solving a system of equations. Work by Kuba [36] inspired many others (for a recent example see [37]) to develop the theory of "switching components". They considered the problem of uniquely reconstructing all entries in a matrix from its directed sums, based initially along the matrix rows and columns. These switching components are structures that prohibit unique inversion. They are equivalent to the Ghosts discussed here.

In recent work, Candès *et al.* [38] showed that an $N \times N$ image can be recovered exactly using convex optimisation of a very small number of projections. However, their method

suffers from high computationally complexity and is still an active area of research [39]. Herman and Davidi [40] discussed the Candès *et al.* [38] result using Ghosts and showed that Ghosts artefacts may still remain invisible to small number of projections when using their method. Nevertheless, their work paves the way in using Ghosts for analysing the sensitivity of reconstruction algorithms. Inspired by their work, the next section constructs a cyclic theory of Ghosts for the Discrete FST.

III. Cyclic Ghosts

In this section, it is shown that Ghosts of the Discrete FST have exact cyclic forms known as m-Circulant matrices (or circulants).

Definition 1 (m-Circulant[1] [41]). *An m-Circulant is an $N \times N$ matrix containing a unique row $f(j)$ with $j = 0, \ldots, N-1$ replicated on each row, but where each row is cyclically shifted $(\bmod N)$ by an additional m elements to the right.*

m-Circulants represent the slices of the Discrete FST via its Fourier "diagonalisation" property. A 2-Circulant is diagonalised by the DFT as illustrated in (5).

$$\begin{bmatrix} \boldsymbol{a_0} & a_1 & a_2 & a_3 & a_4 \\ a_3 & a_4 & \boldsymbol{a_0} & a_1 & a_2 \\ a_1 & a_2 & a_3 & a_4 & \boldsymbol{a_0} \\ a_4 & \boldsymbol{a_0} & a_1 & a_2 & a_3 \\ a_2 & a_3 & a_4 & \boldsymbol{a_0} & a_1 \end{bmatrix} \overset{\text{(i)DFT}}{\Longleftrightarrow} \begin{bmatrix} \lambda_0 & & & & \\ & & \lambda_1 & & \\ & & & & \lambda_2 \\ & \lambda_3 & & & \\ & & & \lambda_4 & \end{bmatrix} \tag{5}$$

The diagonalisation is represented by monomial matrices $\boldsymbol{M} = \boldsymbol{P\Lambda}$, where $\boldsymbol{\Lambda}$ is an $N \times N$ diagonal matrix and $\boldsymbol{P}$ is an $N \times N$ permutation matrix with N non-zero elements representing a discrete line at slope $m \,(\bmod N)$ [41]. Hence, the lines of slope 1 given in part (b) of Fig. 2 is a 1-Circulant. The lines of slope 2 (as in Fig. 2(c)) will be a 2-Circulant and so on.

Every projection can then be represented by an m-Circulant and its 2D DFT represents a slice in discrete Fourier space. Equivalently, since the 1D DFT of the unique circulant row are the diagonal values [41], the 1D DFT of the (1D) projections are the slice values, so that only a computation complexity of $O(N \log_2 N)$ is required to compute each slice. Superimposing a circulant in image space places a slice of corresponding slope in DFT space. The tiling of the diagonals is the same for the lines formed by the vectors $[-m, 1]$ and $[1, -ps]$, so a total of $N + {}^{N}/_{p}$ diagonals is required for full tiling of DFT space. The result is a sum of $N + {}^{N}/_{p}$ circulants in image space to recover the image. This is known as Circulant Back-Projection (CBP) [42] and is illustrated in Fig. 6.

Fill [4] showed that the Discrete FST can be constructed using circulant matrices. Chandra and Svalbe [42] showed that the construction can be extended to other DFT-like transforms, such as the Number Theoretic Transform (NTT). The NTT will be important in removing the cyclic Ghosts exactly (see discussion at the end of this section).

The circulant matrices also allow one to naturally define and understand Ghosts. In what follows, we restrict ourselves to prime-sized image spaces, so that projections are acquired via the vectors $[1, m]$ and $[0, 1]$ with a total of $N + 1$ projections required for an exact reconstruction.

[1] Also referred to as a generalised circulant or g-circulant [41].

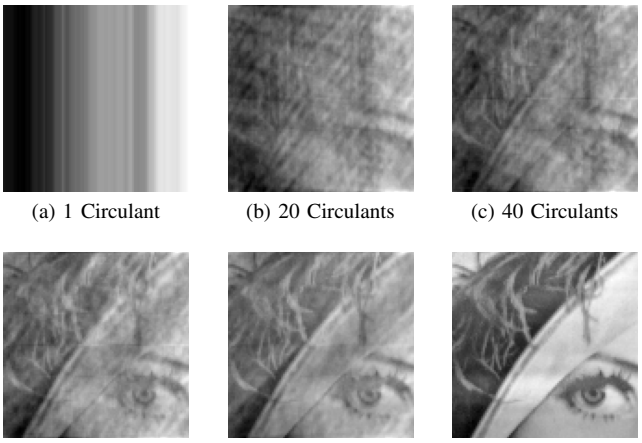

(a) 1 Circulant (b) 20 Circulants (c) 40 Circulants

(d) 60 Circulants (e) 80 Circulants (f) 100 Circulants

Figure 6. Illustration of the CBP of a 101×101 image of Lena using different number of circulants. (a)-(f) show the effect of an increasing number of slices placed into DFT space on the image. The artefacts on the partial reconstructions are cyclic Ghosts.

Proposition 1 (Cyclic Ghosts). *Each missing projection $\boldsymbol{a}'$ at $[1, m_a]$ in the DRT, which corresponds to the missing slice of slope m_a in the DFT, forms artefacts superimposed on the reconstructed image in the form of a m_a-Circulant. The unique row of the circulant is $\boldsymbol{a} = -\boldsymbol{a}'$ and these artefacts are called cyclic Ghosts.*

Proof. When projections are missing, the CBP is incomplete since there must be $N+1$ projections for an exact reconstruction. Each projection is equivalent to a circulant in the reconstruction process. Thus, the remaining missing contributions must be a superposition of $\mathcal{N}$ number of circulants with shifts m_ℓ, where $\ell = 0, \ldots, \mathcal{N}-1$ and $\mathcal{N}$ represents the number of missing projections. The Ghosts are negative-valued since they are missing contributions in the reconstruction. A schematic of the circulant nature of Ghosts is shown in Fig. 7. ◀

Chandra *et al.* [13] showed that given $\mathcal{N}$ redundant or known image rows, $\mathcal{N}$ cyclic Ghosts can be removed exactly by shifting and subtracting redundant rows from the rows that contain image data. Although the algorithm allowed exact recovery of images with missing projections, it required the use of arbitrary precision integers as values grew to the order of 10^{40} when removing just 80-90 Ghosts for large images. The result was an algorithm that had very high computational complexity and one that gave no understanding of the cause of such large values. In the next section, a deconvolution approach is constructed which has a lower computational complexity and shows why such large values arise.

IV. De-Ghosting

This section presents a deconvolution algorithm for removing cyclic artefacts formed from $\mathcal{N}$ missing slices in the Discrete FST. Given $\mathcal{N}$ redundant image rows or columns and a list of unknown projection slopes m_ℓ, a Ghost deconvolution or De-Ghost filter is constructed for an image size N. The filter is then used to deconvolve the Ghost artefacts from the image rows. Note that an open source implementation of all the algorithms

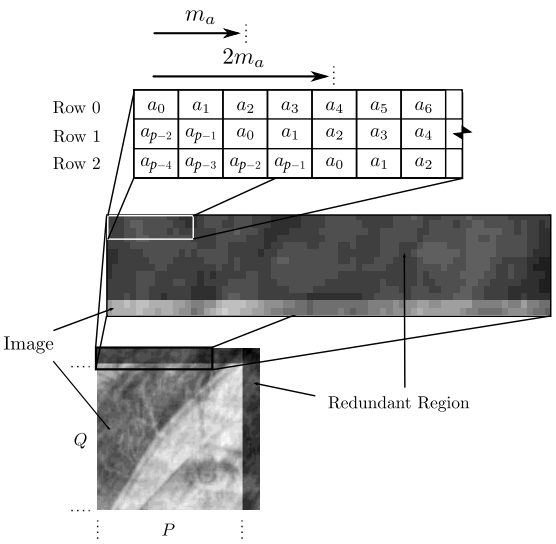

Figure 7. The $Q \times P$ image (Lena) is of 100×100 pixels embedded in a image space $N = 113$ with the remaining pixels equal to zero. Assuming one missing projection $\boldsymbol{a}'$ at $m_a = 2$, then the table shows the circulant artefacts that become embedded over the reconstructed image values (including known areas) where $\boldsymbol{a} = -\boldsymbol{a}'$.

constructed in this paper can be found in the Finite Transform Library written by the authors [43].

Proposition 2 (Ghost Convolution)**.** *Ghosts formed from the missing projections of the DRT are cyclic convolutions of these projections in the geometry of the DFT.*

Proof: According to the Discrete FST, each slice is a cyclic smearing or back-projection of its corresponding projection in image space [4, 42]. Within the geometry of the DFT, convolutions can be represented as a sum of m-Circulants [41]. Thus, the Ghosts that arise due to empty (i.e. zero) projections in the DRT result in an incomplete back-projected image, which are a sum of the missing m-Circulants, and are convolutions in image space. ■

Proposition 3 (Ghost Kernels)**.** *The Ghost convolution kernels required for De-Ghosting are the vectors* $[1, m_j]$*, which sum to zero along its vector for each of the missing projections* $j = 0, \ldots, \mathcal{N} - 1$.

Proof: The projections of Ghosts are zero-valued at their corresponding m-values, so the projection vectors $[1, m_j]$ must also be Ghosts at their m-values in order that Ghosts annihilate with shifted versions of themselves. The kernels apply to each bin in the missing projection or Ghost row (using Prop. 2). An example of a Ghost kernel is shown in Fig. 8(a)-(c). ■

Using Prop. 3, the De-Ghost filter is constructed in the following way:

1) Create a 2D convolution kernel for each unknown slope m_ℓ by placing a $+1$ at the image origin and -1 at $(1, m_\ell)$.
2) Convolve these kernels in 2D to obtain the De-Ghost filter.

The convolution of the kernels may be done either in 2D (in Fourier or image space), or as a set of 1D convolutions on the projections via the Projection Convolution Theorem (PCT) [6] (see Fig. 8). The advantage of the latter is efficiency, especially when the number of known projections $\mu \ll N$.

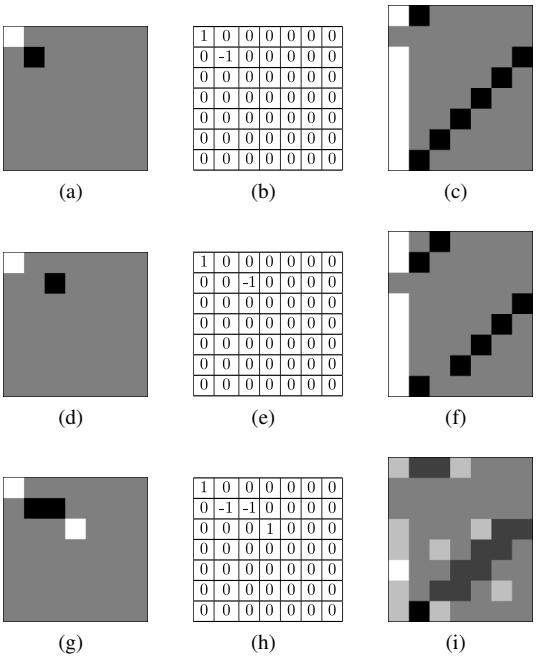

Figure 8. An example of the 1D convolution approach to constructing 2D Ghosts, where grey and black denote zero and minus greyscale values respectively. (a) and (d) show the kernels $[1, 1]$ and $[1, 2]$ respectively. (c), (f) and (i) show the DRT projections of the kernels (a) & (d) and their convolution respectively.

A. Projection Convolution Theorem

The PCT states that a 2D convolution is equivalent to the 1D convolution of each projection or slice in Fourier space. Thus, the 2D Ghost convolution can be computed as a series of 1D convolutions on the known projections. For Ghost convolution, when the number of Ghosts $\mathcal{N}$ is close to N, DRT space is sparse and the 2D convolution is computed over a small number of 1D signals.

The PCT can be interpreted as a consequence of the Discrete FST. Since the slices tile DFT space exactly and are the DFT of the projections, cyclically convolving the slices of two objects is equivalent to cyclically convolving the objects themselves. Thus, in order to utilise the PCT, one needs to know the projections of the two objects. In this case, the projections of the Ghost kernels are particularly convenient, which makes a PCT approach very efficient.

Proposition 4 (Kernel Projections)**.** *The projections of the 2D convolution kernel* $[1, m_\ell]$*, with a positive term at the origin and a negative term at the coordinate* $(1, m_\ell)$*, will have the positive term at the zeroth translate and the negative term at translate* t_j *as*

$$t_j = (m_\ell - m_j) \pmod N \tag{6}$$

for each projection m_j *with* $j = 0, \ldots, N-1$ *and* $\ell = 0, \ldots, \mathcal{N}-1$*. For the* $j = N$ *projection, negative term is always at* $t_j = 1$*. Note that negative values* $-x$ *modulo* N *are equivalent to the value* $N - x \pmod N$.

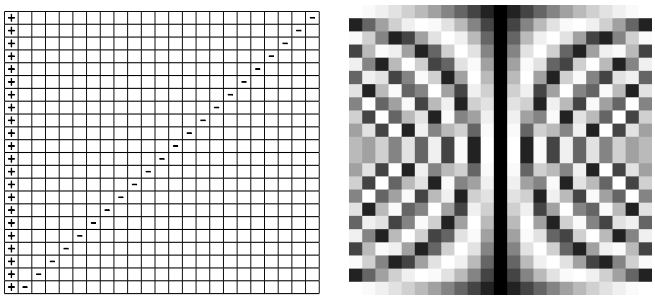

(a) (b)

Figure 9. A schematic of the 1D Ghost convolution operators (a) for $N = 23$. Each row represents the unique projection of a Ghost convolution kernel. (b) shows their eigenvalues in (centred) discrete Fourier space.

Proof. The projection m_ℓ will be zero by definition with all other projections being non-zero. For projections with $m_j < m_\ell$, the negative term will appear in the translates $t > 0 \pmod N$ because the initial vector $[1, m_j]$ for $t = 0$ will not sample the point $(1, m_\ell)$, since slope of the line is smaller than m_ℓ. The difference of slope $(m_\ell - m_j)$ defines the translate where the point is eventually sampled. For projections with $m_j > m_\ell$, the negative term will appear in the translates $t < 0 \pmod N$, i.e. $N - t \pmod N$, because the initial vector $[1, m_j]$ will not sample the point $(1, m_\ell)$ until the vector wraps around the image, since the slope of the line is more than m_ℓ. Hence, the difference of slope $(m_\ell - m_j)$ will be negative and defines the translate where the point is eventually sampled. ◀

Corollary 1 (Kernel Operators)**.** *The projections of the kernels* $[1, m_\ell]$ *only have* N *distinct combinations of positive and negative values.*

Proof. This follows from Prop. 4 and the fact that the system is constructed within a cyclic geometry, i.e. because of the wrapping of the values since there are only N residue classes. ◀

An example of the unique kernel projections (following Cor. 1) and their eigenvalues are shown in parts (a) and (b) of Fig. 9 respectively. These eigenvalues can be precomputed, since they depend purely on the set of slopes of the missing projections as given by Prop. 4. The form of the DFT eigenvalues for $N = 479$ is provided as supplementary material.

Therefore, the 1D Ghost convolution approach may be used to generate a 2D Ghost as follows (see also Fig. 8):

1) Pre-compute the Ghost operator eigenvalues via the DFT for a given N. The results can be used as a hash table to pick out the relevant operator based on the projection being convolved.
2) Convolve a discrete delta function with each of the kernels $[1, m_\ell]$ by selecting the correct eigenvalues for each operator using the eigenvalues hash table (as given by previous step) via Eq. (6) and multiplying these operators with the eigenvalues of the delta function.
3) Repeat the 1D Ghost convolutions for all known projections m_j.
4) Compute the inverse DFT of the result from 3 to obtain the Ghost structure in image space.

The computational complexity is $O(\mathcal{N} N \log_2 N)$ for pre-computing the eigenvalues, $O(\mu N \log_2 N)$ for the 1D DFTs of the known projections and $O(\mu \mathcal{N} N)$ for computing the convolutions. When $\mu \ll N$, the algorithm has a computational complexity of $O(n \log_2 n)$ (where $n = N^2$). However, the convolution is susceptible to round-off errors and loss of precision for large $\mathcal{N}$ when utilising the DFT for the convolutions. This problem, which manifested as numerical overflow, was also encountered by Chandra *et al.* [13] with their method. This numerical growth can be easily seen as a direct consequence of the convolutions of the eigenvalues in Fig. 9. The solution is to use the NTT and the Number-Theoretic Radon Transform (NRT) of Chandra and Svalbe [42].

B. Number Theoretic Convolution

The NTT allows one to compute convolutions using only integers because the unit circle is replaced with the digital "circle"

$$\alpha^{M-1} \equiv 1 \pmod M, \tag{7}$$

so that $\alpha^{M-1} - 1$ is a multiple of M, N is a multiple of $M - 1$ and $\alpha, M \in \mathbb{N}_0$ [44]. The successive powers $\{1, \ldots, M - 1\}$ of α generates a unique set of integers in some order modulo M. Such a number α is called the primitive root. The primitive root(s) α in these cases have to be found by trial and error and can be computed by dividing $M - 1$ by the prime factors p_j of $M - 1$, such that $\alpha^{(M-1)/p_j} \not\equiv 1 \pmod M$, where the trial value of α is prime.

For a prime-length N, the NTT can be computed by first selecting the modulus M as $M = k \cdot N + 1$. This allows the power of α in Eq. (7) to be a multiple of N. For example, the modulus for the prime-length $N = 101$ is 607 with $k = 6$. Then Rader's [45] algorithm can be used to compute its fast form. Integer coefficients allow computations to be done without round-off error or numerical overflow, since the results are congruent modulo M [46].

Chandra and Svalbe [42] showed that the discrete FST still holds within the 2D NTT when placing Number Theoretic slices, i.e. the NTTs of the projections, into 2D NTT space. This allows one to replace the DFT in all computations, including those within the Ghost convolutions, with the NTT. The resulting NRT was constructed specifically to remedy the loss of precision when forming cyclic Ghosts. Chandra and Svalbe [42] also showed that the implementation of the NTT is faster than the DFT because of its integer-only operations. Consequently, the Ghost convolution method is impervious to numerical overflow and faster than DFT approaches.

Ghosts in the NRT have another important property in that any physical or perceivable structures in the Ghosts are difficult to discern. The Ghosts in this space have the value $0 \pmod M$ in the direction of the missing projections. This makes the NRT Ghosts well suited for encoding and encryption. An example of Ghosts within the NRT can be seen in Fig. 10(b). Once the Ghost is constructed/convolved, it can be used to remove the artefacts formed by the missing slices for which it was constructed. This process of De-Ghosting is described in the next section.

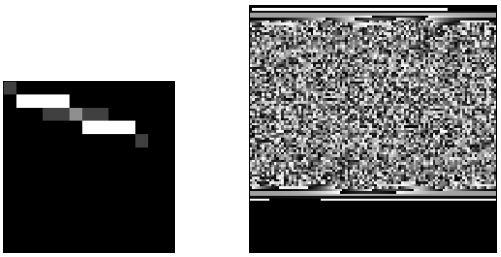

(a) (b)

Figure 10. Examples of Ghosts in the NRT. (a) shows a Ghost with $\mathcal{N} = 4$ at $m = 1, 2, 3, 4 \pmod{53}$, where $N = 13$. (b) shows a Ghost with $\mathcal{N} = 80$ at $m = 1, \ldots, 80 \pmod{607}$, where $N = 101$.

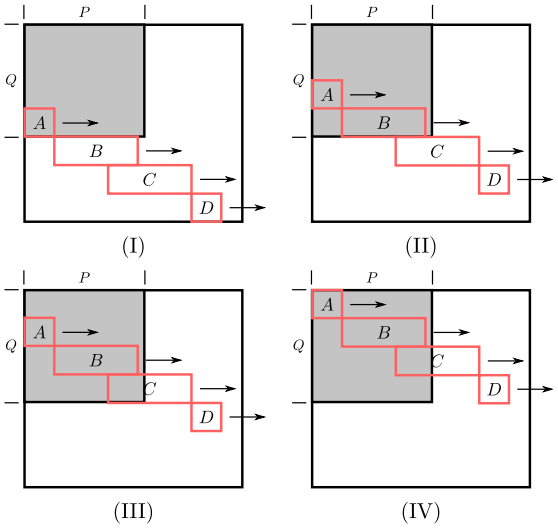

Figure 11. A De-Ghost example for a $Q \times P$ image (in grey), where a row of the De-Ghost filter (in red) is aligned to an image row $\tilde{I}(3, 0)$ (with the remaining filter rows in redundant space) and the row-wise 1D convolution of the filter (with the Ghosted image rows) recovers the image row $\tilde{I}(3, 0)$. The result is back-substituted to create a redundant row and the process repeated, as in (II), (III) and (IV), to recover the image.

C. Ghost Deconvolution

The Ghost constructed in the previous section may be applied as an exact deconvolution mask/filter to recover the missing slices of the Discrete FST. The filter is aligned to an image row to be De-Ghosted and the deconvolution computed in one of two ways.

A simple but inefficient deconvolution method is to zero-pad the sub-image that contains the image row to be recovered, as well as the required $\mathcal{N}$ redundant rows, within the $N \times N$ space and compute the 2D convolution with the filter. A more efficient approach is to individually convolve each row of the filter with the corresponding row of the image as shown in Fig. 11. The result of each 1D convolution would then need to be summed to the image row being recovered. For example, the sum of convolutions in Fig. 11(I) is effectively a sub-circulant expression given as

$$\boldsymbol{A} \cdot \tilde{I}(3, 0)^T + \boldsymbol{B} \cdot \tilde{I}(4, 0)^T + \boldsymbol{C} \cdot \tilde{I}(5, 0)^T + \boldsymbol{D} \cdot \tilde{I}(6, 0)^T = I(3, 0)^T, \tag{8}$$

where $\tilde{I}$ denotes the Ghosted image, I denotes the desired De-Ghosted sub-image and the matrices $\boldsymbol{A}, \boldsymbol{B}, \boldsymbol{C}$ and $\boldsymbol{D}$ are circulants defined by the rows A, B, C and D of the filter in Fig. 11. These circulants represent the 1D convolutions of the rows of the filter. The resultant image row is back-substituted and the filter translated up or down to recover the next row. In this case, row $I(3, 0)$ is back-substituted into $\tilde{I}(3, 0)$ in order to make it a redundant row and the filter is translated upwards to the next row and Eq. (8) is repeated for (II). The process is repeated for all image rows until all the Ghosts are removed.

In the 1D convolution method, the m-values of the Ghosts need to be $-m_\ell$ (i.e. $N - m_\ell$ rather than m_ℓ) when convolving the Ghosts to undo the right shift of the m-Circulants. A total of $\mathcal{N} + 1$ rows need to be convolved, resulting in a computational complexity of $O(Q\mathcal{N}N)$. When $\mu = \min(P, Q) + 1$ and $\mu \ll N$, the algorithm has a computational complexity of $O(n \log_2 n)$ (where $n = N^2$). A visual interpretation to constructing Ghosts, that unifies the Ghost recovery algorithm of Chandra *et al.* [13], Latin squares approach of Chandra and Svalbe [14] and the 2D convolution approach of this paper, can be made using n-gons (see the thesis of Chandra [47]).

More work has to be done with both methods when the projections or slices contain noise or inconsistencies as these also become convolved during the De-Ghost process. The convolution approach requires a very good estimation of noise prior to De-Ghosting, so that the estimates may be used to deconvolve their effects on the results. Future work includes generalising the approach to arbitrary missing discrete Fourier coefficients. Recent work by Svalbe *et al.* [48–50] discussed the minimal extent of cyclic Ghosts, which may prove useful in this endeavour. In the next section, the De-Ghost method is applied to the discrete inverse problem of determining a reconstruction from a set of highly asymmetric rational angle projections.

V. Application: Discrete Reconstruction

Chandra *et al.* [13] utilised their Ghost removal technique to exactly reconstruct an image from rational angle (noise-free) discrete 1D projections of the MT. The projections sets in their work required covering the half-plane, i.e. the interval $[0, \pi)$. In this section, the De-Ghost method will be applied to reconstructing from a set of rational angle projections with arbitrary coverage of the half-plane, such as those within a quadrant or the interval $[0, \pi/2)$, provided there are $\min(P, Q) + 1$ projections for a $Q \times P$ image. Both sets require that the projections satisfy the Katz criterion (4) for exact reconstruction.

In the De-Ghost reconstruction algorithm, a $Q \times P$ image is zero padded into an $N \times N$ space, where $N \geqslant \max(P, Q)$. A total of $\min(P, Q) + 1$ projections are required to ensure that the number of redundant image rows is equal to the number of missing slices $\mathcal{N}$, since there will be $N + 1$ slices within DFT space. An efficient new method for generating $\min(P, Q) + 1$ highly asymmetric rational angles is presented in the Appendix. Assuming that $\min(P, Q) + 1$ of this type of projections have been acquired, the remaining parts of this section will demonstrate the performance of the De-Ghost algorithm in reconstructing these rational angle projections exactly, where a large number of Ghosts are present.

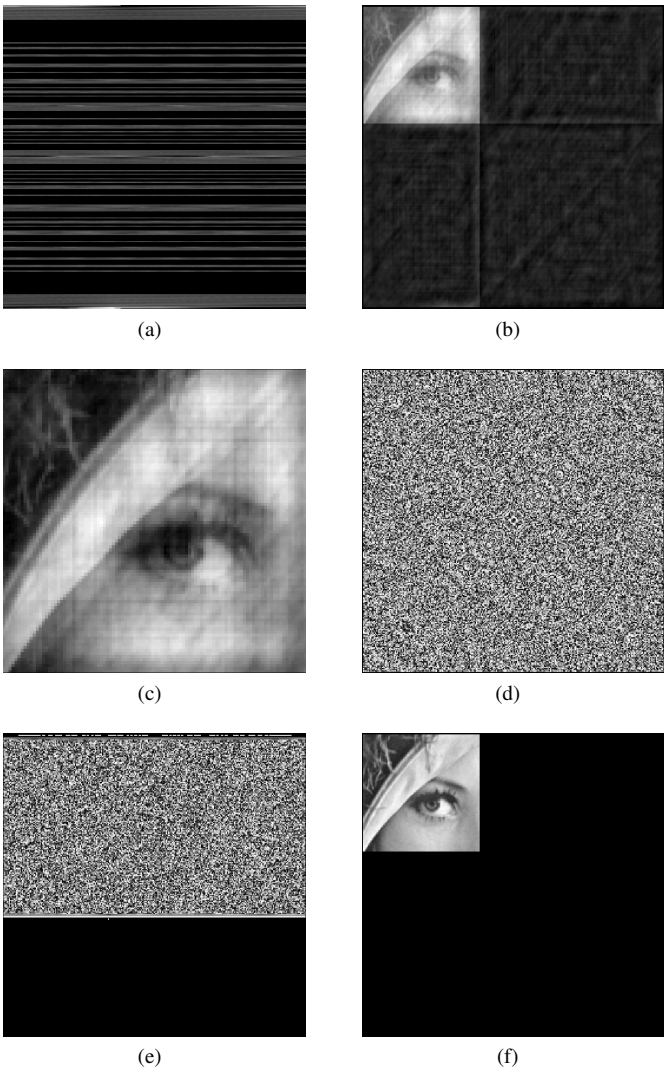

Figure 12. The results of the De-Ghost method applied to discrete reconstruction. A total of 101 asymmetric rational angle projections of a 100×100 image of Lena was exactly reconstructed within a DFT space of size 257×257. (a) shows the resulting DRT space. (b) shows the resulting Ghosts when (a) is reconstructed. (c) shows a cropped version of (b) focussing on the embedded image. (d) and (e) show the Ghost eigenvalues and the Ghost that was used to recover the reconstructed image exactly (shown in (f)).

Consider a 100×100 image of Lena and 101 rational angle projections similar to the geometry of Fig. 14(a). Also let $N = 257$ for performance purposes, so that $N - 1$ is a power of two. Thus, there will be 156 Ghosts to remove and also 156 redundant rows in the image, so that the De-Ghost method can be applied.

Fig. 12(a) shows the DRT space resulting from 101 rational projections acquired across the quadrant and mapped via Eq. (9). Fig. 12(b) and (c) show the resulting Ghosts superimposed on the reconstruction due to the missing projections in (a). Fig. 12(d) shows the NTT Ghost eigenvalues that are used to construct the deconvolution Ghost in Fig. 12(e). Fig. 12(f) shows the final result of the De-Ghosting, which is an exact reconstruction. The computation time was approximately 500 milliseconds on a single-core 1.6 GHz AMD Turion™ 64-bit Laptop. This algorithm performs several orders of magnitude faster than the method of Chandra *et al.* [13], whose computations took in the order of hours to complete on the same machine.

Further work needs to be done to handle inconsistencies within projections while utilising De-Ghosting. Also, a study of the small variations within the rational angle multiplicity may be critical in understanding whether some projections are more "important" than others. The information in an image is known to be distributed non-uniformly amongst its discrete projections. The variance for a DRT projection m, with equivalent MT projection $[b, a]$, scales inversely as $(a^2 + b^2)$.

Conclusion

A theory for missing slices of the Discrete FST was constructed that allowed description of Ghost artefacts in the 2D DFT. The theory was used to construct new Ghost convolution and deconvolution methods, having a computational complexity of $O(n \log_2 n)$ with $n = N^2$, which can be utilised in recovering missing slices in the DFT (see Props 1 to 4). The methods required the use of the NTT in order to avoid numerical overflow and loss of precision problems. This De-Ghost method was then used to solve the discrete inverse problem of reconstructing exactly from highly asymmetric rational angle projections (see Figs 12 and 14).

Acknowledgements

S. Chandra would like to thank Monash University for a Ph.D scholarship and a publications award. N. Normand would like to thank the Australian Research Council for his International Fellowship (ARC LX 0989907).

Appendix
Ghost Angle Sets

Chandra *et al.* [51] showed that any MT projection, acquired along a rational vector $[b, a]$, can be directly and efficiently mapped to a prime-sized DFT space exactly as

$$m \equiv ab^{-1} \pmod{N}, \tag{9}$$

where $a, b \in \mathbb{Z}$ with $\gcd(a, b) = 1$ and b^{-1} is the multiplicative inverse of b. The mapping (9) results from solving $mb \equiv a \pmod{N}$. Each Mojette bin or translate $t_{\mathcal{M}}$ is then placed into a DRT translate $t_{\mathcal{R}}$ as

$$t_{\mathcal{R}} = \begin{cases} b^{-1}\ t_{\mathcal{M}} \pmod{N}, & \text{if} \quad \gcd(a, N) > 1 \\ a^{-1}\ t_{\mathcal{M}} \pmod{N}, & \text{if} \quad \gcd(b, N) > 1 \end{cases}. \tag{10}$$

An efficient way to generate the values a and b is to minimise the L_1-norm of the rational vectors $[b, a]$. This can be computed as

$$b_3 = \left\lfloor \frac{b_1 + a_1 + N}{a_2} \right\rfloor b_2 - b_1, \quad a_3 = \left\lfloor \frac{b_1 + a_1 + N}{a_2} \right\rfloor a_2 - a_1, \tag{11}$$

where $\lfloor \cdot \rfloor$ is the floor (round-down) operator, beginning the computation with $[b_1, a_1] = [0, 1]$ and $[b_2, a_2] = [1, N]$ until $[b_3, a_3] = [1, 1]$ [51]. Positive $[b, a]$ values represent the first octant of the half-plane with the other octants produced by $[-b, a], [a, b]$ and $[a, -b]$ vectors [16]. The resulting m values from these rational vectors can be compared with values

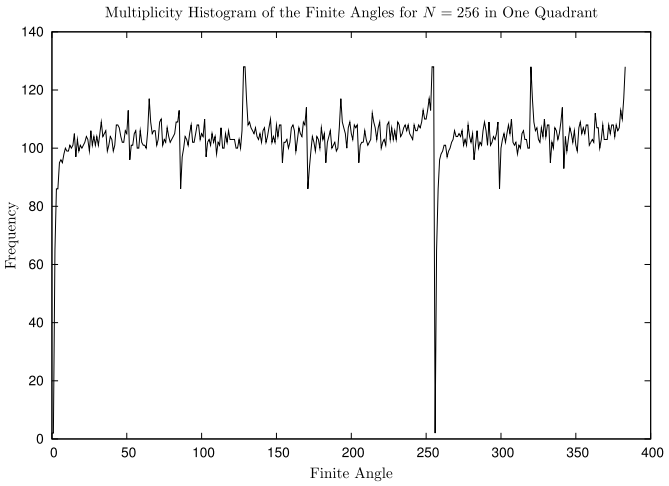

Figure 13. The multiplicity of the mapping between the finite angle and rational angle sets for $N = 256$, i.e. for the dyadic case. Because of the dyadic size, the range of values are $0 \leqslant m < N$ and $s' = N + s$, where $0 \leqslant s < N/2$.

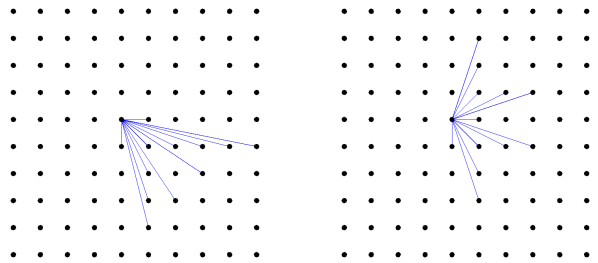

Figure 14. Examples of rational projection sets when utilising Ghosts in discrete reconstruction. (a) shows a set limited to a quadrant and (b) shows a set using the half-plane. The sets apply to a 11×11 image embedded into a 23×23 space.

previously computed to obtain the desired DFT coverage. Eq. (11) produces rational angles that result in more compact projections in terms of the number of bins B, since

$$B = |a|(Q-1) + |b|(P-1) + 1. \tag{12}$$

Minimising L_1-norm of the rational angles allows one to acquire $N+1$ projections of certain coverage with reduced redundancy. The De-Ghost methods discussed in this work does not depend on how the rational angles are generated or selected.

This method can be extended to cover a fraction of the half-plane by limiting the number of octants used within the projection set. One then can obtain a set that sparsely covers the half-plane, but one that can still completely cover DFT space. This is because there exists a multiplicity of possible rational vectors for each finite angle $[1, m]$ across the half-plane. The multiplicity is a consequence of the one-to-many nature of the m rational mapping in Eq. (9). A total of $\min(P, Q) + 1$ projections can then be selected from this set that satisfies Katz criterion (4), while still being highly asymmetric. This multiplicity is shown as graphs in Fig. 13 for a single quadrant and the half plane.

The multiplicity of the m rational mapping appears to be relatively "flat" in a discrete sense, but with small variations. Graph 13 is reminiscent of curves obtained by Svalbe and Kingston [52] when observing the "unevenness" of the rational vectors from uniform coverage. The unevenness of the rational vectors is related to the distribution of prime numbers and the Riemann hypothesis [53]. Once $\min(P, Q) + 1$ projections are chosen, the theory of cyclic Ghosts can be applied to reconstruct these projections exactly. It effectively reduces the number of projections required to $\min(P, Q) + 1$, rather than a total $N+1$ in the traditional case. Examples of each projection set are given in Fig. 14.

References

[1] A. Grigoryan, "New algorithms for calculating the discrete Fourier transforms," *J. Vichislit. Matem. i Mat. Fiziki*, vol. 25, no. 9, pp. 1407–1412, 1986.

[2] E. D. Bolker, "The Finite Radon Transform," *Contemporary Mathematics (American Mathematical Society)*, vol. 63, pp. 27–49, 1987.

[3] I. Gertner, "A new efficient algorithm to compute the two-dimensional discrete Fourier transform," *Acoustics, Speech and Signal Processing, IEEE Transactions on*, vol. 36, no. 7, pp. 1036–1050, Jul 1988.

[4] J. A. Fill, "The Radon Transform on $\mathbb{Z}_n$," *SIAM Journal on Discrete Mathematics*, vol. 2, no. 2, pp. 262–283, 1989.

[5] G. T. Herman and A. Kuba, *Discrete tomography: foundations, algorithms, and applications*. Birkhäuser, 1999.

[6] F. Matúš and J. Flusser, "Image Representation via a Finite Radon Transform," *Pattern Analysis and Machine Intelligence, IEEE Transactions on*, vol. 15, no. 10, pp. 996–1006, 1993.

[7] A. Kingston and I. Svalbe, "Generalised finite Radon transform for NxN images," *Image and Vision Computing*, vol. 25, no. 10, pp. 1620 – 1630, 2007, Discrete Geometry for Computer Imagery 2005.

[8] T. Hsung, D. Lun, and W.-C. Siu, "The discrete periodic Radon transform," *Signal Processing, IEEE Transactions on*, vol. 44, no. 10, pp. 2651–2657, 1996.

[9] D. Lun, T. Hsung, and T. Shen, "Orthogonal discrete periodic Radon transform. Part I: theory and realization," *Signal Processing*, vol. 83, no. 5, pp. 941–955, 2003.

[10] ——, "Orthogonal discrete periodic Radon transform. Part II: applications," *Signal Processing*, vol. 83, no. 5, pp. 957–971, 2003.

[11] A. Kingston, "Orthogonal discrete Radon transform over $p^n \times p^n$ images," *Signal Processing*, vol. 86, no. 8, pp. 2040 – 2050, 2006, special Section: Advances in Signal Processing-assisted Cross-layer Designs.

[12] M. Katz, *Questions of Uniqueness and Resolution in Reconstruction from Projections*, ser. Lecture Notes in Biomathematics. Springer-Verlag, 1977.

[13] S. S. Chandra, I. Svalbe, and J.-P. Guédon, "An exact, non-iterative Mojette inversion technique utilising ghosts," in *Lecture Notes in Computer Science (LNCS)*. Springer Berlin / Heidelberg, 2008, vol. 4992, pp. 401–412.

[14] S. S. Chandra and I. Svalbe, "A method for removing cyclic artefacts in discrete tomography using Latin squares," *19th International Conference on Pattern Recognition*, pp. 1–4, Dec. 2008.

[15] N. Normand, I. D. Svalbe, B. Parrein, and A. M. Kingston, "Erasure coding with the finite Radon transform," in *IEEE Wireless Communications & Networking Conference*, Sydney, Apr. 2010.

[16] I. Svalbe, "Exact, scaled image rotation using the Finite Radon Transform," *Pattern Recognition Letters*, vol. 32, no. 9, pp. 1415–1420, 2011.

[17] R. N. Bracewell and J. A. Roberts, "Aerial Smoothing in Radio Astronomy," *Australian Journal of Physics*, vol. 7, pp. 615–640, Dec. 1954.

[18] T. Cornwell, "Image Restoration and the Clean Technique," in *Synthesis Mapping*, A. R. Thompson & L. R. D'Addario, Ed., 1982, p. 9.

[19] A. K. Louis, "Ghosts in tomography - the null space of the Radon transform," *Mathematical Methods in the Applied Sciences*, vol. 3, pp. 1–10, 1981.

[20] B. F. Logan, "The uncertainty principle in reconstructing functions from projections," *Duke Mathematical Journal*, vol. 42, no. 4, pp. 661–706, 1975.

[21] G. N. Ramachandran and A. V. Lakshminarayanan, "Three-dimensional Reconstruction from Radiographs and Electron Micrographs: Application of Convolutions instead of Fourier Transforms," *Proc. of the Nat. Acad.*

of Sciences, vol. 68, no. 9, pp. 2236–2240, 1971.
[22] L. Shepp and B. Logan, "The Fourier reconstruction of a head section," *Nuclear Science, IEEE Transactions on*, vol. 21, pp. 21–43, 1974.
[23] A. C. Kak and M. Slaney, *Principles of Computerized Tomographic Imaging*. Society of Industrial and Applied Mathematics, 2001.
[24] A. K. Louis, "Nonuniqueness in inverse Radon problems: The frequency distribution of the ghosts," *Mathematische Zeitschrift*, vol. 185, no. 3, pp. 429–440, 1984.
[25] J.-P. Guédon, D. Barba, and N. Burger, "Psychovisual image coding via an exact discrete Radon transform," *Proc. of the SPIE - The International Society for Optical Engineering*, vol. 2501, pp. 562–572, 1995.
[26] N. Normand, A. Kingston, and P. Évenou, "A geometry driven reconstruction algorithm for the Mojette transform," in *Lecture Notes in Computer Science (LNCS)*. Springer Berlin / Heidelberg, 2006, vol. 4245, pp. 122–133.
[27] N. Normand, J.-P. Guédon, O. Philippe, and D. Barba, "Controlled redundancy for image coding and high-speed transmission," *Proc. of the SPIE - The International Society for Optical Engineering*, vol. 2727, pp. 1070–1081, 1996.
[28] J.-P. Guédon, N. Normand, A. Kingston, B. Parrein, M. Servières, P. Évenou, I. Svalbe, F. Autrusseau, T. Hamon, Y. Bizais, D. Coeurjolly, F. Boulos, and E. Grail, *The Mojette Transform: Theory and Applications*. ISTE-Wiley, 2009.
[29] M. Servières, J. Idier, N. Normand, and J.-P. Guédon, "Conjugate gradient Mojette reconstruction," *Proc. of the SPIE - The International Society for Optical Engineering*, vol. 5747, no. 1, pp. 2067–2074, 2005.
[30] J. Boyd and J. Little, "Complementary data fusion for limited-angle tomography," *Proc. 1994 IEEE Computer Society Conference on Computer Vision and Pattern Recognition*, pp. 288–294, 1994.
[31] D. L. Donoho and P. B. Stark, "Uncertainty principles and signal recovery," *SIAM Journal on Applied Mathematics*, vol. 49, p. 906, 1989.
[32] D. L. Donoho and B. F. Logan, "Signal recovery and the large sieve," *SIAM Journal on Applied Mathematics*, vol. 52, p. 577, 1992.
[33] D. L. Donoho, "For most large underdetermined systems of linear equations the minimal ℓ_1-norm solution is also the sparsest solution," *Communications on Pure and Applied Mathematics*, vol. 59, no. 6, pp. 797–829, 2006.
[34] J. Wright and Y. Ma, "Dense Error Correction Via ℓ^1-Minimization," *Information Theory, IEEE Transactions on*, vol. 56, no. 7, pp. 3540 –3560, july 2010.
[35] M. Vetterli, P. Marziliano, and T. Blu, "Sampling signals with finite rate of innovation," *IEEE Transactions on Signal Processing*, vol. 50, no. 6, pp. 1417–1428, Jun. 2002.
[36] A. Kuba, "The reconstruction of two-directionally connected binary patterns from their two orthogonal projections," *Computer vision, graphics, and image processing*, vol. 27, no. 3, pp. 249–265, 1984.
[37] S. Brunetti, P. Dulio, and C. Peri, "Characterization of -1, 0, +1 valued functions in discrete tomography under sets of 4 directions," in *Lecture Notes in Computer Science (LNCS)*, vol. 6607, 2011, pp. 394–405.
[38] E. Candès, J. Romberg, and T. Tao, "Robust uncertainty principles: exact signal reconstruction from highly incomplete frequency information," *Information Theory, IEEE Transactions on*, vol. 52, no. 2, pp. 489–509, February 2006.
[39] A. Ganesh, Z. Lin, J. Wright, L. Wu, M. Chen, and Y. Ma, "Fast algorithms for recovering a corrupted low-rank matrix," in *Comp. Adv. in Multi-Sensor Adaptive Processing (CAMSAP), IEEE International Workshop on*, 2009, pp. 213 –216.
[40] G. Herman and R. Davidi, "Image reconstruction form a small number of projections," *Inverse Problems*, vol. 24, p. 17, 2008.
[41] P. J. Davis, *Circulant Matrices*. John Wiley & Sons, 1979.
[42] S. S. Chandra and I. D. Svalbe, "Exact image representation via a Number-Theoretic Radon Transform," *IET Computer Vision*, 2012, accepted.
[43] S. S. Chandra, "The Finite Transform Library (FTL)," Monash University, Australia, Available at SourceForge.net, C/C++ Library (Open Source under GPL v3) 1.0, 2009. [Online]. Available: http://finitetransform.sourceforge.net
[44] J. M. Pollard, "The Fast Fourier Transform in a Finite Field," *Mathematics of Computation*, vol. 25, no. 114, pp. 365–374, 1971.
[45] C. M. Rader, "Discrete Fourier transforms when the number of data samples is prime," *Proceedings of the IEEE*, vol. 56, no. 6, pp. 1107–1108, June 1968.
[46] H. J. Nussbaumer, "Overflow detection in the computation of convolutions by some number theoretic transforms," *Acoustics, Speech and Signal Processing, IEEE Transactions on*, vol. 26, no. 1, pp. 108–109, Feb 1978.
[47] S. S. Chandra, "Circulant Theory of the Radon Transform," Ph.D. dissertation, School of Physics, Monash University, 2010, Online Monash ARROW Repository.
[48] I. Svalbe, N. Normand, N. Nazareth, and S. S. Chandra, "On constructing minimal ghosts," *Proceedings of the Digital Image Computing Techniques and Applications (DICTA)*, pp. 276 – 281, 2010.
[49] I. Svalbe and N. Normand, "Properties of minimal ghosts," in *Lecture Notes in Computer Science (LNCS)*. Springer Berlin / Heidelberg, 2010, vol. 6607, pp. 417–428.
[50] I. Svalbe and S. S. Chandra, "Growth of discrete projection ghosts created by iteration," in *Lecture Notes in Computer Science (LNCS)*, I. Debled-Rennesson, E. Domenjoud, B. Kerautret, and P. Even, Eds. Springer Berlin / Heidelberg, 2011, vol. 6607, pp. 406–416.
[51] S. S. Chandra, N. Normand, A. Kingston, J.-P. Guédon, and I. Svalbe, "Fast Mojette Transform for Discrete Tomography," *Journal of Mathematical Imaging and Vision*, 2010, submitted December (in Review), Available on arXiv:1006.1965v1 [physics.med-ph].
[52] I. Svalbe and A. Kingston, "On correcting the unevenness of angle distributions arising from integer ratios lying in restricted portions of the Farey plane," *Combinatorial Image Analysis. 10th International Workshop, IWCIA 2004. Proceedings (LNCS)*, vol. 3322, pp. 110–121, 2004.
[53] J. Franel, "Les suites de farey et le problème des nombres premiers," *Göttinger Nachrichten*, pp. 191–201, 1924.

Shekhar S. Chandra was born in Suva, Fiji Islands in 1980. He received a B.Sc. in computer science at the University of the South Pacific (Fiji), followed by a B.Sc. (Hons) in physics at Monash University (Australia) and a Ph.D in physics at Monash University (Australia) in 2010.

He is currently a post-doctoral fellow at the Australian e-Health Research Centre, CSIRO, where he is undertaking research in medical imaging. His current research interests include image/signal processing, number theory, biomedical imaging and discrete tomography.

Imants D. Svalbe was born in Ballarat, Australia, in 1952. He received the B.Sc. (Hons) degree in physics in 1974 and the Ph.D. degree in nuclear physics, in 1979, both from the University of Melbourne, Australia.

He is currently a Senior Lecturer in the School of Physics at the Clayton Campus of Monash University, Australia, where he teaches physics and medical imaging to radiography students. His principal research interests are focussed on discrete effects in digital image processing. He has spent several periods as an Invited Visiting Professor at the University of Nantes, and is currently an Associate Editor for Pattern Recognition Letters.

Andrew M. Kingston was born in Brisbane, Australia in 1978. He received a B.Sc. degree in 1999 and a B.Eng. (Hons.) degree in 2002 at Monash University. He was awarded a Ph.D in physics at Monash University in 2006.

He is currently a Research Fellow in the Department of Applied Mathematics in the Research School of Physics and Engineering at the Australian National University. Prior to that he held a Post-Doctoral position at the IRCCyN laboratory in Ecole polytechnique de l'universite de Nantes. His research interests are centered around computed tomography and the associated Radon transform (both continuous and discrete forms).

Jeanpierre Guédon was born in Grosbreuil, France in 1962. He received the M.S degree and Ph.D degree from Ecole Centrale de Nantes and University of Nantes in 1986 and 1990 respectively, working on sampling in tomography with Yves Bizais. In 1991-92, he was a post-doc at CDRH FDA Rockville MD, USA with Kyle Myers and Bob Wagner. In 1994, he was assistant professor at Polytech Nantes then professor since 2002.

He developed the Mojette transform with several colleagues since 1994. His fields of interest concerns the theory around the Mojette transform and its numerous applications for storing and transmissions and for medical imaging. He invented the Mojette game in 2010.

Nicolas Normand was born in Nantes, France, in 1969. He received the Dipl.Ing. degree from INSA, Rennes, in 1992, the M.S. degree from the University of Nantes in 1993 and the Ph.D degree in computer science from the University of Nantes in 1997.

He has been holding a permanent position (Maître de Conférences) at the IRCCyN laboratory in Polytech Nantes, formerly IRESTE, since 1997. In 2009, he was awarded an International Fellowship grant ARC LX0989907 from the Australian Research Council and spent 12 months in the School of Physics, Monash University, Melbourne. His research fields of interest are discrete tomography, especially the Mojette transform and discrete Radon transform, and discrete distances.